Hydrogen Gas Production from the Injection of Nanoscale Zero-Valent Iron and Sodium Borohydride Solutions: Potential Effects Near Injection Wells

Obai Mohammed
obai.mohammed@queensu.ca
Queen's University, Kingston, Ontario
Current address: Technical Support Section, Ministry of the Environment, Conservation and Parks, Kingston, Ontario

Kevin G. Mumford
kevin.mumford@queensu.ca
Queen's University, Kingston, Ontario

Brent E. Sleep
sleep@efc.utoronto.ca
University of Toronto, Toronto, Ontario

ABSTRACT

The injection of nano-scale zero-valent iron (nZVI) is a remediation technique for the treatment of organic and metal contamination in soil and groundwater. The hydrogen gas (H2) produced during the reaction of nZVI and excess sodium borohydride (NaBH4) used in nZVI synthesis with water can inhibit nZVI transport in the subsurface, potentially limiting solution delivery to the target contaminant zone. Laboratory experiments were completed in a thin flow cell using NaBH4 and nZVI solutions injected into water-saturated medium sands, in which local gas saturations were quantified using a light transmission technique to calculate H2 gas volumes. Hydraulic conductivity, under water-saturated and quasi-saturated conditions, after gas exsolution and throughout gas dissolution, was measured. The results showed that H2 gas volume produced as a result of the reaction of nZVI with water was more than the H2 gas volume produced by the self-hydrolysis of NaBH4 solution regardless of similar NaBH4 concentration used as excess during nZVI synthesis. Pools of H2 gas were formed after injecting nZVI prepared with excess 5 g/L NaBH4 or after injecting 5 g/L NaBH4 without nZVI. Gas accumulated predominantly in a vertical layer of coarse sand, illustrative of a sand pack surrounding an injection well. Lower hydraulic conductivity measurements were linked to higher gas saturations and further reductions were evident as a result of gas pool accumulation at the top of the flow cell. These results show that gas production during the application of nZVI is an important process that must be considered during remediation design and operation to ensure effective delivery to target zones.

Keywords: Nano-scale zero-valent iron (nZVI); Volatile organic compounds; Light transmission

1 INTRODUCTION

In situ chemical reduction with nZVI is a promising technology for the treatment of source-zone and dissolved chlorinated solvents in the groundwater and subsurface soils. Yet, the application of nZVI is challenged by the reduced nZVI solution mobility during injection in some subsurface environments (He et al., 2009). In addition to

concerns regarding agglomeration and sedimentation of nZVI, H_2 gas produced during nZVI implementation can cause changes in groundwater flow patterns (Johnson et al., 2013). Figure 1 is a graphical representation of an nZVI application where H_2 gas exolves during the reaction of nZVI with water near the injection area. In the treatment area, the nZVI reacts with water and volatile organic compounds (VOCs) in the non-aqueous phase liquid (NAPL) source, producing H_2 gas and VOCs that can be mobilized upwards, possibly causing contaminant relocation to the location above the injection area.

Previous field studies have reported complications with nZVI mobility, despite the modification of nZVI with polymers and surface coatings (Kocur et al., 2014, 2013). This indicates that nZVI mobility may be limited for reasons other than nano-particle stability. H_2 gas exsolving from the reaction of freshly synthesized nZVI with water (Chen et al., 2011) is a potential cause of this limitation. Mohammed et al. (2019) performed bench-scale experiments to quantify and determine the consequences of H_2 gas exsolving uniformly during the self-hydrolysis reaction of $NaBH_4$ solution with deionized water in silica sands packed in an acrylic flow cell. Their results showed lower hydraulic conductivity values linked to increased gas saturations associated with increased $NaBH_4$ solution concentrations. Mohammed et al. (2019) concluded that H_2 gas production could decrease the hydraulic conductivity if high concentrations of $NaBH_4$ are added for nZVI synthesis during field application. It is anticipated that nZVI injections will also be affected by heterogeneity in the immediate proximity of an injection well (i.e., the sand pack) which can create a preferential location for gas accumulation.

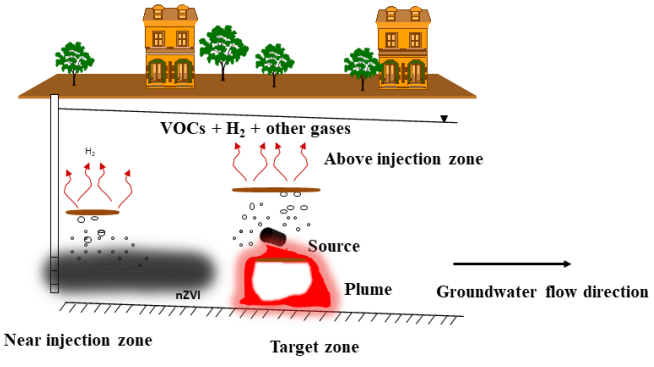

Figure 1: Simplified schematic of a nZVI field injection

In this study H_2 gas exsolving from the nZVI reaction with water compared to $NaBH_4$ self-hydrolysis reaction with water was visualized and quantified, and images were examined to determine the potential of gas mobilization in each case. In addition, the potential effect of H_2 gas exsolution on the effective hydraulic conductivity was investigated, and reductions in hydraulic conductivity were measured as H_2 gas dissolved from a vertical high-permeability layer, representative of a sand pack around a field injection well.

2 MATERIALS AND METHODS

Experiments were completed at the bench-scale by injecting $NaBH_4$ and nZVI solutions into homogeneous medium sand packs. Silica Accusand 20/30 and 12/20 grades, with median particle diameters (d_{50}) of 0.713 mm and 1.105 mm (Schroth et al., 1996), and porosity values of 0.38 and 0.37 to 0.38 (Mohammed et al., 2019), respectively, were used for the experiments performed in a thin acrylic flow cell. Four injection experiments, including two $NaBH_4$ and two nZVI solutions were performed at room temperature (21° C). H_2 gas was produced by the self-hydrolysis of $NaBH_4$, and by nZVI reaction with water. Hydraulic conductivity measurements were determined under water-saturated conditions before gas exsolution, directly after gas exsolution in all experiments, and throughout H_2 gas dissolution. H_2 gas saturations were quantified using a light transmission method.

2.1 Flow Cell

A 22 cm × 34 cm × 1 cm acrylic flow cell (Figure 2), equipped with a top seal to sustain confined conditions, and two clear-wells promoting horizontal water flow, was used to perform the experiments. The flow cell had four bottom drainage ports with water-wet hydrophilic nylon membranes (10 μm pore size, EMD Millipore Corporation) installed to facilitate drainage of sand packs to a residual wetting saturation. A model TJE low range wet-wet (Honeywell International Inc.) differential pressure transducer, attached through water-filled tubes to the clear-wells, was used to measure the differential pressure during the flowing part of the experiments, and the differential pressure data were logged throughout each experiment using a HOBO UX120-006M Analog data logger (Onset Computer Corporation). A vertically oriented layer of 12/20 silica Accusand was packed in the first 6 cm measured from the left inflow clear-well boundary and the remaining part of the cell was packed with 20/30 silica Accusand. This configuration was used to represent a coarse sand pack neighboring an injection well in field applications. In order to remove fines, all sands were washed with deionized water and packed as a slurry into the cell, which was half-way filled with deionized water to create a water-saturated condition to begin with.

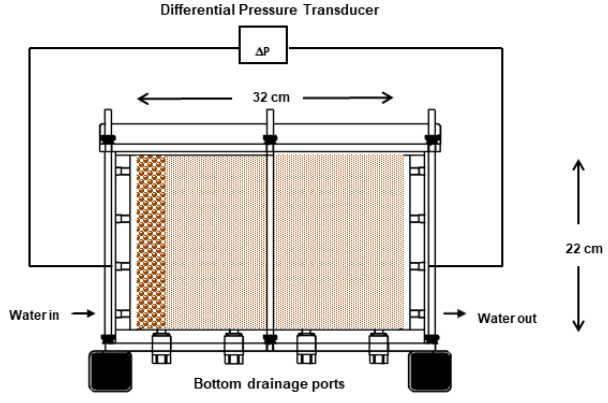

Figure 2: Flow cell sketch

2.2 Gas Visualization and Quantification

A light transmission technique (Tidwell and Glass, 1994; Niemet and Selker, 2001; Mumford et al., 2015; Mohammed et al., 2019) was used to visualize and quantify H_2 gas saturations. Gas saturations(S_g) were calculated from light intensities (I) transmitted through water-saturated conditions (I_s) and residual conditions (I_r). The method assumes uniform diameter pores that are either filled with water or filled with gas and a residual film of water. Effective wetting saturations of an image (I) were calculated using (Niemet and Selker, 2001):

$$S_e = \frac{\ln(I)-\ln(I_r)}{\ln(I_s)-\ln(I_r)} = 1 - \frac{\ln(I/I_s)}{\ln(I_r/I_s)} \quad (1)$$

where I is the light intensity transmitted through the sand, and I_s and I_r are the light intensities transmitted through a fully water-saturated or a residual saturated sand, respectively. Gas saturation was then calculated as:

$$S_g = 1 - (S_e(1 - S_{wr}) + S_{wr}) \quad (2)$$

where S_{wr} is the residual wetting saturation, measured in independent experiments (Mohammed et al., 2019). A light emitting diode (LED) panel (Led Go, CN-1200H) was used as the light source and a single-lens reflex digital camera (Canon, EOS Rebel T3i) was used to capture the images throughout the experiments. The light transmission setup was covered with a black fabric to avoid changes in light while experiments were conducted and the camera settings were held constant.

2.3 Solutions Injection

A volume of 10 mL of $NaBH_4$ or nZVI solution was injected in the flow cell through the left-hand clear-well near the 12/20 Accusand portion of the sand pack. $NaBH_4$ solution concentrations of 1.25 g/L and 5 g/L were carefully chosen since they are representative of concentrations used for 1 g/L nZVI synthesis by means of 2:1 to 4:1 excess $NaBH_4$ ratio described in recent laboratory experiments and field investigation trials (Boparai et al., 2011; Kocur et al., 2013). The nZVI concentration of 1 g/L used during injection experiments has also been reported in field applications and bench-scale experiments (Kocur et al., 2014, 2013; Stefaniuk et al., 2016). The $NaBH_4$ concentrations in experiments E-1 and E-2 correspond to the excess $NaBH_4$ concentrations used for nZVI synthesis in experiments E-3 and E-4 to allow direct comparison between pairs of experiments (Table 1). The experiments were conducted mainly in two parts. The first part (exsolution) was conducted in a static batch mode, with no water flowing through the cell (E-1 to E-4). During gas exsolution, water was displaced out of the cell through one open outflow port, and was recorded using a laboratory balance (Mettler Toledo MS6002S with Mettler Toledo LabX Direct software). Images were captured throughout exsolution every 2 to 5 minutes. The gas volumes calculated from the digital images were obtained by considering the 12/20 and 20/30 sand packed areas separately during image processing and summed to get the total H_2 gas volume. Gas volumes calculated from the captured images using light transmission were related to the displaced water volumes to obtain a best-fit value of (I_r/I_s) in Equation 1 (Mumford et al., 2015; Mohammed et al., 2019). In the second part of each experiment (water flow), deionized water was pumped

through the sand packs at 36.8 mL/min, equivalent to a pore water velocity of 4.4 cm/min (F-1 to F-4). The measured pressure difference between the inflow and outflow boundaries was used to calculate the effective hydraulic conductivity across the entire flow cell. The flow rate was selected to produce high pressure drops with measurable differences between water-saturated and exsolved gas conditions, but was maintained within the Darcy flow regime with Reynolds number of 0.5 in the 20/30 Accusand. The water flow part was sustained for 12.5 to 19 pore volumes for experiments F-3 and F-4, but continued for 189 to 225 pore volumes for experiments F-1 and F-2, respectively (Table 1), to further examine the dissolution of H_2 gas trapped within the 12/20 Accusand (i.e., the coarse sand pack).

Table 1: Solution injection experiments

Exsolution	Water flow	$NaBH_4$ (g/L)	nZVI (g/L)	Pore-volumes Flushed
E-1	F-1	1.25	-	189.0
E-2	F-2	5.00	-	225.0
E-3	F-3	1.25*	1.0	14.0
E-4	F-4	5.00*	1.0	18.0

*excess $NaBH_4$ used during nZVI synthesis

3 RESULTS AND DISCUSSION

3.1 Gas Exsolution

Exsolved gas volumes in the four experiments are shown in Figure 3. $NaBH_4$ solution was used in experiments E-1 and E-2, and nZVI solution (which includes excess $NaBH_4$) was used in experiments E-3 and E-4. The best-fit values of (I_r/I_s) in the 12/20 and the 20/30 sand packed experiments E-1 to E-4 were found to be 0.79 ± 0.03 and 0.58 ± 0.06, respectively, consistent with 0.69 and 0.56 I_r/I_s values reported by (Mohammed et al., 2019) using a similar light transmission set-up and image processing technique. The lower concentration $NaBH_4$ solutions or nZVI solutions synthesized with lower $NaBH_4$ concentrations (E-1 and E-3) produced less H_2 gas compared to injecting higher concentration $NaBH_4$ solutions or nZVI solutions synthesized with higher concentrations of $NaBH_4$ (E-2 and E-4) (Figure 3). This is consistent with the findings reported by Mohammed et al. (2019). Importantly, similar $NaBH_4$ solution concentrations produced more H_2 gas when paired with nZVI. The H_2 gas exsolution rate decreased with increasing time in all experiments (Mohammed et al., 2019). Gas volumes reached a plateau after 250 min in experiment E-1, but did not reach a plateau after greater than 600 min in experiment E-2, which used a higher $NaBH_4$ concentration. In contrast, gas volumes reached a plateau after 100 min in experiment E-3, and 200 min in experiment E-4, which also used a higher $NaBH_4$ concentration in excess for nZVI synthesis (Figure 3). This shorter time to reach the plateau in the nZVI injection experiments (E-3 and E-4) was expected due to the high reactivity of the nanoparticles associated with high nZVI surface area. A relatively similar reaction time for H_2 exsolution from nZVI of about two hours was reported by (Huang et al., 2016).

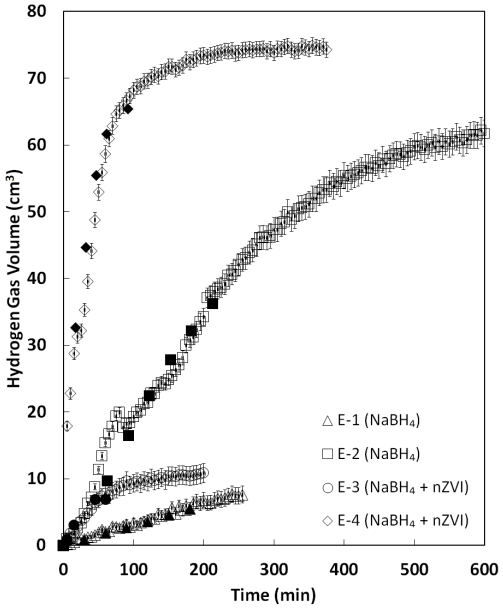

Figure 3: H_2 gas volume produced with time. Open symbols signify volumes of H_2 gas calculated by image processing and closed symbols signify the volumes of gas equivalent to the displaced water volumes during H_2 gas exsolution.

3.2 H_2 Gas Production and Mobilization

Figure 4 illustrates the distribution of gas images processed for gas saturations at different times as H_2 exsolved throughout the experiments. Consistent behavior is evident in all of the performed experiments. H_2 gas is produced mainly in the coarse sand (12/20 Accusand) near the clear-well in which the solution is injected. In all experiments, the volume of gas exsolved was sufficiently high to result in buoyant gas mobilization, resulting in higher gas saturations at the top of the coarse sand. Intermediate gas saturations were also evident at the bottom of the coarse sand, due to exsolution from injected solution that was transported downwards due to its higher density. The lowest gas saturations occurred in the middle of the coarse sand due to gas exsolution and trapping. At later time, H_2 gas progressed into the 20/30 Accusand pack, either driven by gas invasion at the top or by the exsolution of gas from the dense solution at the bottom. In experiments E-2 and E-4, where higher $NaBH_4$ solution concentrations were injected, higher gas saturations and mobilized gas formed a gas pool at the top of the coarse sand that was able to enter and advance to form a gas pool in the finer 20/30 sand. In experiment E-2, this gas pool in the finer sand was also supplied by discontinuous gas flow from the bottom of the finer sand pack as the gas saturations increased due to the self-hydrolysis of $NaBH_4$ (gas fingers in Figure 4g,h). Although high concentrations were also used in experiment E-4, there was no gas mobilization in the finer sand pack in that experiment. This is attributed to the high reactivity of nZVI, resulting in nearly all of the H_2 gas being formed within the first hour and close to the coarse sand compared to the hydrolysis reaction that lasted more than 2 hours.

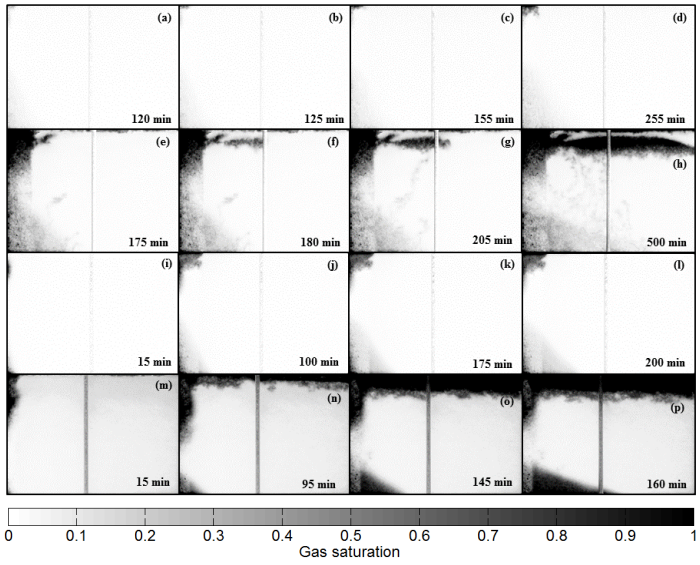

Figure 4: Selected gas saturation images showing H_2 gas exsolution and mobilization from (a)–(d) Experiment E-1, (e)–(h) Experiment E-2, (i)–(l) Experiment E-3, and (m)–(p) Experiment E-4

3.3 Hydraulic Conductivity and Flow

The non-uniform distribution of gas, both vertically and laterally, resulted in substantial spatial variation in aqueous phase relative permeability. The overall relative permeability value (i.e., at the scale of the flow cell) is used here to describe the effect of gas produced in the experiments. The hydraulic conductivity under water-saturated conditions (experiments F-1 to F-4) was 29.8 ± 2.0 cm/min (mean ± one standard deviation). Following H_2 gas exsolution in experiments F-1 and F-3, the hydraulic conductivity was reduced to 26.9 ± 0.3 cm/min and 27.5 ± 0.2 cm/min. This reduction in hydraulic conductivity was associated with H_2 gas volumes of 7.7 ± 1.2 and 11.5 ± 1.4 cm^3, respectively. Replicate experiments conducted under water-saturated conditions were used to calculate standard deviation values in all of the exsolution experiments with the assumption of a constant coefficient of variation based on previously conducted air entrapment and exsolution experiments (Mohammed et al., 2019) used to measure effective hydraulic conductivity. Further reductions in hydraulic conductivity were related to increased $NaBH_4$ solution concentrations (experiments F-2 and F-4). Reduced hydraulic conductivity values of 17.0 ± 3.1 cm/min and 24.1 ± 2.1 cm/min were caused by larger H_2 gas volumes of 62.2 ± 2 and 74.9 ± 1.2 cm^3, respectively. These reductions correspond to overall aqueous phase relative permeability values of 0.62-0.94. However, based on the gas distribution (Figure 4) the reduction in hydraulic conductivity is controlled by large reductions in aqueous phase relative permeability in the coarse sand pack, particularly near the top of the pack for high-concentration injections. As a result, of H_2 gas dissolution due to water flow up to 189 pore volumes in experiment F-1, the hydraulic conductivity value bounced back steadily to the value measured under water-saturated conditions. Yet, dissolution of H_2 gas in experiment F-2 was able to return the

hydraulic conductivity value to only 22.9 ± 0.1 cm/min (82% of the value under water-saturated conditions), even after flushing 225 pore volumes of water through the sand pack. The gas accumulated at the top of the cell in the form of a gas pool exhibited slow dissolution (Figure 4h), with local gas saturations up to 67% remaining.

4 CONCLUSION

The experiments conducted in this study demonstrated that H_2 gas exsolution from the reaction of nZVI prepared with excess $NaBH_4$ with water was more than the H_2 gas exsolved due to the self-hydrolysis of $NaBH_4$ solution alone, despite similar concentrations of $NaBH_4$. Increasing $NaBH_4$ solution concentration resulted in more H_2 gas production, whether the increased $NaBH_4$ solution concentration is injected alone, or is used during nZVI synthesis. Most of the gas exsolved within the coarser sand representative of a sand pack surrounding an injection well, and was mobilized upwards by buoyancy. However, additional gas was produced at the bottom of the sand pack, due to the downward transport of the injected solution driven by density. Vertically mobilized gas channels were created as a result of nZVI solution injection prepared with excess 5 g/L $NaBH_4$ concentration, but was also created in the experiment in which 5 g/L $NaBH_4$ solution was injected alone. In both experiments where 5 g/L $NaBH_4$ was used, the produced gas created H_2 gas pools. Exsolved H_2 gas caused a reduction in the effective hydraulic conductivity, with higher gas saturations resulting in lower effective hydraulic conductivities. Gradual increases in hydraulic conductivity were measured during H_2 gas dissolution, although it did not return to the water-saturated hydraulic conductivity in both experiments due to gas persistence.

In field-scale nZVI applications, H_2 gas produced during the injection of nZVI prepared with excess $NaBH_4$ upstream of a contaminant zone can reduce nZVI mobility and inhibit delivery to the target contaminant zone by blocking pores and reducing the effective hydraulic conductivity, with more reduction expected when using higher concentrations of $NaBH_4$ during nZVI synthesis due to additional H_2 gas production. Gas mobilization can also result in gas pool formation should low permeability layers exist in the injection application area, further decreasing the effective hydraulic conductivity. These impacts can be more severe due to exsolution in the sand pack in the vicinity of the injection well screens, in which H_2 gas can be mobilized upwards in the coarse sand, creating gas pools at the upper portion of the sand pack. While some gas from these pools may flow back into the injection well, depending on the entry pressure of the well screen and the height of the sand pack above the well screen, residual gas that remains in the sand pack will limit subsequent injections. Given that the sand pack is coarser than the surrounding porous medium by design, it is a preferential location for gas accumulation, with the amount of accumulation subject to the displacement pressure of the sand nearby. In these experiments, more than 120 pore volumes of water were required to dissolve the H_2 gas produced by exsolution. This suggests that flow limitations and flow diversion could extend for longer time periods in a field application, including between consecutive nZVI injections. Persistent redirection of groundwater flow is detrimental if repeated nZVI solution injections to the target zone are deemed necessary. Flow diversion can also complicate the analysis of groundwater sampling data collected downgradient if the results are compared to pre-injection conditions.

REFERENCES

Boparai, H. K., Joseph, M., O'Carroll, D. M. (2011). Kinetics and thermodynamics of cadmium ion removal by adsorption onto nano zerovalent iron particles. J. Hazard, *Mater*, 186, 458-465. DOI: 10.1016/j.jhazmat.2010.11.029.

Chen, K. F., Li, S. & Zhang, W. (2011). Renewable hydrogen generation by bimetallic zero valent iron nanoparticles. *Chem. Eng. J.*, 170, 562-567. DOI: 10.1016/j.cej.2010.12.019.

He, F., Zhao, D. & Paul, C. (2010). Field assessment of carboxymethyl cellulose stabilized iron nanoparticles for in situ destruction of chlorinated solvents in source zones. *Water Res*., 44, 2360-2370. DOI: 10.1016/j.watres.2009.12.041.

Huang, Y. X., Guo, J., Zhang, C. & Hu, Z. (2016). Hydrogen production from the dissolution of nano zero valent iron and its effect on anaerobic digestion. *Water Res*., 88, 475-480. DOI: 10.1016/j.watres.2015.10.028.

Johnson, R. L., Nurmi, J. T., O'Brien Johnson, G. S., Fan, D., O'Brien Johnson, R. L. & Shi, Z. et al. (2013). Field-scale transport and transformation of carboxymethylcellulose-stabilized nano zero-valent iron. *Environ. Sci. Technol*., 47:1573-1580. DOI: 10.1021/es304564q.

Kocur, C. M., Chowdhury, A. I., Sakulchaicharoen, N., Boparai, H. K., Weber, K. P., Sharma, P., Krol, M. M., Austrins, L., Peace, C., Sleep, B. E. & O'Carroll, D. M. (2014). Characterization of nZVI mobility in a field scale test. *Environ. Sci. Technol*., 48, 2862-2869. DOI: 10.1021/es4044209.

Kocur, C. M., O'Carroll, D. M. & Sleep, B. E. (2013). Impact of nZVI stability on mobility in porous media. *J. Contam. Hydrol.,* 145, 17-25. DOI: 10.1016/j.jconhyd.2012.11.001.

Mohammed, O., Mumford, K. G. & Sleep, B. E. (2019). Relative permeability measurements during the exsolution and dissolution of hydrogen gas produced by the hydrolysis of sodium borohydride. *Vadose Zone J*., 18:190043. DOI: 10.2136/vzj2019.04.0043.

Mumford, K. G., Hegele, P. R. & Vandenberg, G. P. (2015). Comparison of Two-Dimensional and Three-Dimensional Macroscopic Invasion Percolation Simulations with Laboratory Experiments of Gas Bubble Flow in Homogeneous Sands. *Vadose Zo. J.*, 14. DOI: 10.2136/vzj2015.02.0028.

Niemet, M. R. & Selker, J. S. (2001). A new method for quantification of liquid saturation in 2D translucent porous media systems using light transmission. *Adv. Water Resour.*, 24, 651-666. DOI: 10.1016/S0309-1708(00)00045-2.

Schroth, M.H., Istok, J. D., Ahearn, S. J., Selker, J. S., 1996. Characterization of Miller-Similar Silica Sands for Laboratory Hydrologic Studies. *Soil Sci. Soc. Am. J*., 60, 1331. DOI: 10.2136/sssaj1996.03615995006000050007x.

Stefaniuk, M., Oleszczuk, P. & Ok, Y. S. (2016). Review on nano zerovalent iron (nZVI): From synthesis to environmental applications. *Chem. Eng. J*., 287, 618-632. DOI: 10.1016/j.cej.2015.11.046.

Tidwell, V. C. & Glass, R. J. (1994). X ray and visible light transmission for laboratory measurement of two-dimensional saturation fields in thin-slab systems. *Water Resour. Res*., 30, 2873-2882. DOI: 10.1029/94WR00953.

Cite this article as: Mohammed O., Mumford K. G., Sleep B. E., "Hydrogen Gas Production from the Injection of Nanoscale Zero-Valent Iron and Sodium Borohydride Solutions: Potential Effects Near Injection Wells", *International Conference on Civil Infrastructure and Construction (CIC 2020)*, Doha, Qatar, 2-5 February 2020, DOI: https://doi.org/10.29117/cic.2020.0090